Structural Safety 49 (2014) 45–55

Contents lists available at ScienceDirect

Structural Safety

journal homepage: www.elsevier.com/locate/strusafe

Effect of spatially variable shear strength parameters with linearly increasing mean trend on reliability of infinite slopes

Dian-Qing Li [a], Xiao-Hui Qi [a], Kok-Kwang Phoon [b], Li-Min Zhang [c], Chuang-Bing Zhou [a,*]

[a] State Key Laboratory of Water Resources and Hydropower Engineering Science, Wuhan University, 8 Donghu South Road, Wuhan 430072, PR China
[b] Department of Civil and Environmental Engineering, National University of Singapore, Blk E1A, #07-03, 1 Engineering Drive 2, Singapore 117576, Singapore
[c] Department of Civil and Environmental Engineering, The Hong Kong University of Science and Technology, Clear Water Bay, Kowloon, Hong Kong

ARTICLE INFO

Article history:
Available online 15 November 2013

Keywords:
Soil slopes
Slope stability
Shear strength
Spatial variability
Random field
Reliability

ABSTRACT

This paper studies the reliability of infinite slopes in the presence of spatially variable shear strength parameters that increase linearly with depth. The mean trend of the shear strength parameters increasing with depth is highlighted. The spatial variability in the undrained shear strength and the friction angle is modeled using random field theory. Infinite slope examples are presented to investigate the effect of spatial variability on the depth of critical slip line and the probability of failure. The results indicate that the mean trend of the shear strength parameters has a significant influence on clay slope reliability. The probability of failure will be overestimated if a linearly increasing trend underlying the shear strength parameters is ignored. The possibility of critical slip lines occurring at the bottom of the slope decreases considerably when the mean trend of undrained shear strength is considered. The linearly increasing mean trend of the friction angle has a considerable effect on the distribution of the critical failure depths of sandy slopes. The most likely critical slip line only lies at the bottom of the sandy slope under the special case of a constant mean trend.

1. Introduction

Slope stability is a typical problem in geotechnical engineering (e.g., [3,26,33]). It is well known that soil is a complex engineering material that has been formed by a combination of various geologic, environmental, and physio-chemical processes. Because of these natural processes, all soil properties in situ will vary vertically and horizontally [27]. Hence, a realistic assessment of slope reliability should consider the spatial variability of shear strength parameters [1,6].

Different aspects of spatial variability of shear strength parameters on slope reliability have been studied in the past (e.g., [15,12,24,32,8,16,13,17,40,41]). For example, Hicks and Samy [15] studied the influence of heterogeneity of undrained shear strength on the stability of a clay slope. Griffiths and Fenton [12] studied the effect of spatial variability of the undrained shear strength on the probability of failure of a slope. Low et al. [24] proposed a practical EXCEL procedure to analyze slope reliability in the presence of spatially varying shear strength parameters. Srivastava and Sivakumar Babu [32] quantified the spatial variability of soil parameters using field test data and evaluated the reliability of a spatially varying frictional/cohesive soil slope. Cho [8] investigated the effect of spatial variability of shear strength parameters accounting for the correlation between cohesion and friction angle on slope reliability. Hicks and Spencer [16] conducted a reliability analysis of a long 3D clay slope. The influence of spatial heterogeneity on the failure mode was studied. Griffiths et al. [13] performed a probabilistic analysis to explore the influence of spatial variation of shear strength parameters on the reliability of infinite slopes. Ji et al. [17] adopted the First Order Reliability Method (FORM) coupled with a deterministic slope stability analysis to search for the probabilistic critical slip surface when spatial variability of shear strength parameters is considered. Zhu et al. [41] explored the variance of matric suction and factor of safety of a slope subjected to steady-state rainfall infiltration in the presence of spatially varying shear strength parameters.

In the majority of these studies, the spatial variability of shear strength parameters was modeled as a stationary random field. In other words, the means of the shear strength parameters are constant with depth. However, it is well recognized that a soil property fluctuates about a trend that typically increases with depth [27]. The fluctuating component is viewed as the inherent soil variability, while the trend function is viewed as the mean of the soil property at various depths. Many in-situ test data revealed that soil properties of a statistically homogeneous soil layer did exhibit non-constant trends with depth [2,15,10,11,18,31,32,5,36,29,37,38]. For example, Wilson et al. [36,37] investigated the undrained stability of circular and square tunnels where the shear strength

* Corresponding author. Tel./fax: +86 27 6877 4295.
E-mail addresses: dianqing@whu.edu.cn (D.-Q. Li), kkphoon@nus.edu.sg (K.-K. Phoon), cbzhou@whu.edu.cn (C.-B. Zhou).

0167-4730/$ - see front matter © 2013 Elsevier Ltd. All rights reserved.
http://dx.doi.org/10.1016/j.strusafe.2013.08.005

increases linearly with depth. Wu et al. [38] studied the reliability of basal heave stability of deep excavations in which the undrained shear strength varies with depth. Hence, while the detrended fluctuations can be modeled as a zero-mean stationary random field, the actual value of the soil property consisting of the trend and the fluctuation is generally non-stationary (in the mean) and this effect should be studied in slope reliability problems.

This paper aims to study the reliability of infinite slopes in the presence of spatial varying shear strength parameters that increase linearly with depth on the average. To achieve this goal, this article is organized as follows. In Section 2, the mean variation of shear strength parameters with depth is discussed. In Section 3, the spatial variabilities in the undrained shear strength and the effective stress friction angle are modeled by random fields, which are discretized by Karhunen-Loeve (KL) expansions. In Section 4, a method to determine the reliability of infinite slopes is presented. In Section 5, infinite slope examples are analyzed to study the effect of spatial variability in the presence of a linearly increasing mean trend on the most likely depth of the critical slip line and the probability of failure. Discussions on shallow landslides related to spatial variability are presented in Section 6.

2. Spatial variability of soils

2.1. Trend of undrained shear strength with depth

The undrained shear strength is often used for undrained stability analysis of clay slopes. It is well known that the undrained shear strength is not a fundamental soil parameter, and its value depends on the effective confining stress, among others. An increase in effective confining stress generally causes an increase in undrained shear strength. For slightly plastic and medium plastic soil, the undrained shear strength, s_u, can be expressed as [19]:

$$s_u/\sigma'_v = (0.23 \pm 0.04)\mathrm{OCR}^{0.8} \tag{1}$$

where σ'_v is the effective vertical stress which can be calculated by $\sigma'_v = \gamma' Z$, in which γ' denotes the effective unit weight of the soil and z denotes the depth below the ground surface. The OCR is the overconsolidation ratio, which is defined as:

$$\mathrm{OCR} = \sigma'_p/\sigma'_v \tag{2}$$

where σ'_p is the effective preconsolidation stress, which is the maximum vertical effective stress experienced by a point in a soil mass in the past. If the present ground surface is defined as $z = 0$ and the maximum overburden depth in the past is d, σ'_p at any given depth z would be $\gamma'(z + d)$. In this case, Eq. (2) can be written as:

$$\mathrm{OCR} = (z + d)/z \tag{3}$$

For normally consolidated soil, OCR is equal to 1. For overconsolidated soil, OCR usually lies between 1 and 50. For highly plastic soil, the undrained shear strength depends not only on the effective vertical stress and the overconsolidation ratio, but also on the plasticity index [19].

Eq. (1) is adopted to characterize the depth trend of the undrained shear strength in an approximate but realistic way. The following parameters are adopted: $\gamma' = 10$ kN/m^3, $d = 35$ m, and the maximum value of the OCR is capped at 50. The lower and upper bounds of s_u are calculated using Eq. (1), i.e. lower bound = $0.19\mathrm{OCR}^{0.8}$ and upper bound = $0.27\mathrm{OCR}^{0.8}$. Fig. 1 shows the variation of these lower and upper bounds with depth. A simple linear trend falling within these bounds is selected in this study (i.e. the line with triangle marker in Fig. 1). Asaoka and A-Grivas [2] also pointed out that s_u can increase linearly with depth from a non-zero value for overconsolidated soils. This conclusion is consistent with the simple model adopted in this study. A vertical line

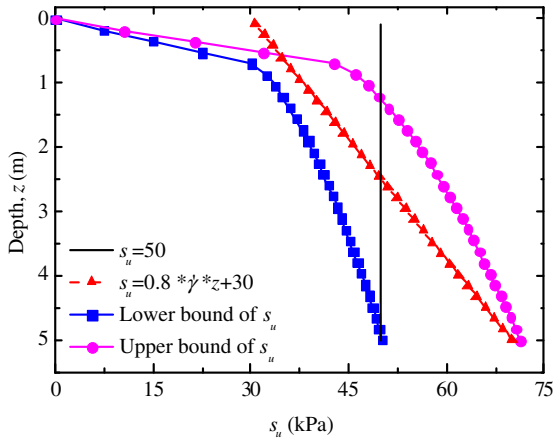

Fig. 1. Trend of undrained shear strength of overconsolidated soil with depth.

representing a constant $s_u = 50$ kPa scenario is also plotted in Fig. 1. This vertical line has been widely used in geotechnical engineering practice due to its simplicity (e.g. [12,8,16,13,17]). It is evident that the resulting undrained shear strength significantly exceeds the upper bound of s_u when the depth is less than 1.2 m. Although this difference looks minor, it can be important for shallow landslides.

2.2. Trend of effective friction angle with depth

Unlike the undrained shear strength, the effective friction angle is a more fundamental soil parameter. For brevity, the effective friction angle is referred to as the friction angle from hereon. The trend function of friction angle with depth is not widely reported in the literature, possibly because undisturbed sand samples are difficult to obtain.

In this paper, some in-situ test data and an empirical relation between friction angle and in-situ test data are used to estimate a reasonable trend function for the friction angle. The following empirical relation for sand is adopted in this study. It relates the friction angle with the cone tip resistance measured in a cone penetration test (CPT) [19]:

$$\phi = 17.6 + 11.0\log_{10}\left(\frac{q_c/p_a}{\sqrt{\sigma'_v/p_a}}\right) \tag{4}$$

in which ϕ is the friction angle of sand; q_c is the cone tip resistance, and p_a is the standard atmospheric pressure ≈100 kPa.

To characterize the trend of friction angle with depth using Eq. (4), CPT data for sandy soils at four different sites are used. Based on these data, the ϕ-z functions can be obtained using Eq. (4) as shown in Fig. 2. Note that $\gamma' = 10$ kN/m^3 is adopted for calculating σ'_v in Fig. 2(a, b, d) because the sandy soil layers are below the ground water table while $\gamma' = 20$ kN/m^3 is adopted in Fig. 2(c) because the ground water table is very deep at the site. It can be seen that the friction angle increases with depth. This is consistent with the trend of friction angle of fine to medium-grained sand layer in Nakdong River Delta [30]. The normalization using σ'_v in Eq. (4) does not remove the depth trend in the CPT data, although it is tempting to think that this will happen and the friction angle can be assumed to be constant along depth. It should be pointed out that there also exists a trend of friction angle decreasing with depth due to the reduced dilatancy of sand with increasing stress level. However, only the case of friction angle of sandy soil increasing with depth is investigated in this study for consistency. Moreover, since all the q_c data in Fig. 2 are collected from field cone penetration tests, it is reasonable to assume that the trend of

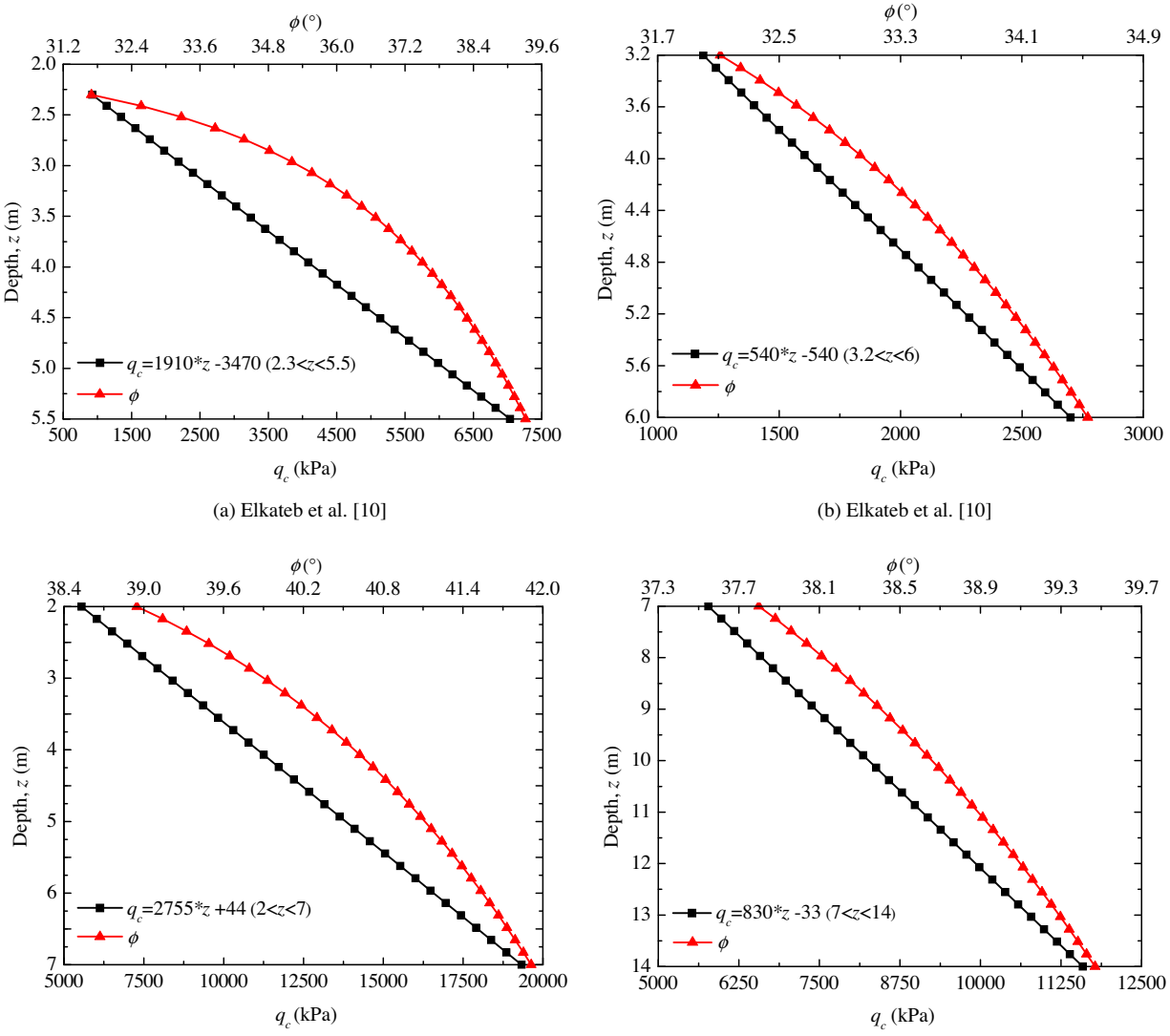

Fig. 2. Trend of friction angle with depth.

friction angle increasing with depth does exist in geotechnical practice.

3. Simulation of spatial variability of shear strength parameters

Several methods such as the midpoint method, the local average subdivision (LAS) method, the shape function method and the KL expansion method can be used to discretize the random field (e.g., [35]). For computational efficiency, the KL expansion is used to simulate the spatial variability of shear strength parameters.

3.1. Simulation of undrained shear strength

As discussed in Section 2.1, the undrained shear strength is likely to increase linearly with depth for overconsolidated soils as follows:

$$s_u = a\sigma'_v + b = a\gamma' z + b \tag{5}$$

where a is the rate of change of the mean undrained shear strength with depth; b is the mean value of the undrained shear strength at the ground surface ($z = 0$). A large value of a will result in a significant difference in the undrained shear strength at various depths; a small value of a will produce an almost constant profile. Values of a and b can be estimated using the linear regression approach (e.g., [35]). These values are not widely reported in the literature, possibly because they are site-specific and therefore not of general interest. This study adopts a linear trend that falls between the lower and upper bounds of the undrained shear strength as shown in Fig. 1. In addition, the coefficient of variation (COV) of unit weight of soils is below 0.1 [27]. Hence, it can be treated as a deterministic value rather than a random variable. The parameter b is also considered to be deterministic for simplicity. The spatial variability of s_u is modeled by treating the parameter a as a homogeneous random field [38]. The mean and standard deviation of s_u are respectively given by:

$$\begin{cases} t_{su}(z) = \mu_a \sigma'_v + b = \mu_a \gamma' z + b \\ \sigma_{su}(z) = COV_a \mu_a \sigma'_v = COV_a \mu_a \gamma' z \end{cases} \tag{6}$$

in which $t_{su}(z)$ and $\sigma_{su}(z)$ are the mean and standard deviation of s_u; μ_a is the mean of a; COV_a is the COV of a which is the ratio of the

standard deviation of a to the mean of a. The COV of s_u, COV_{su}, can be derived as

$$COV_{su} = \frac{COV_a \mu_a \gamma'}{\mu_a \gamma' + b/z} \tag{7}$$

As for the distribution of a, Lacasse and Nadim [20] suggested that both normal and lognormal distributions can be approximately used for describing a. To avoid negative values, the marginal distribution of a is considered to be a lognormal distribution. Hence, the mean and standard deviation of the natural logarithm of a are respectively given by [22,7]:

$$\begin{cases} \lambda_{\ln a} = \ln(\mu_a) - 0.5\ln(1 + COV_a^2) \\ \xi_{\ln a} = \sqrt{\ln(1 + COV_a^2)} \end{cases} \tag{8}$$

in which $\lambda_{\ln a}$ and $\xi_{\ln a}$ are the mean and standard deviation of the natural logarithm a. The simulation steps are given elsewhere [39].

The autocorrelation function is an important parameter for characterizing a random field. For simplicity and convenience [8], a common single exponential autocorrelation function is adopted for $\ln(a)$ as follows:

$$\rho(z_1, z_2) = \exp\left(-\frac{|z_1 - z_2|}{l_v}\right) \tag{9}$$

where ρ is the correlation coefficient between $\ln(a(z_1))$ and $\ln(a(z_2))$; z_1 and z_2 are depth coordinates; l_v is the correlation length of $\ln(a)$ in the depth direction. For slope reliability analysis with a slope height H, the correlation length is commonly represented in a normalized form $\Delta = l_v/H$. As pointed out by Wu et al. [38], the correlation length of a is conceptually the same as that of the undrained shear strength.

Fig. 3 shows the measured s_u–z curve based on CPT data reported in [14] and three simulated s_u–z curves using the parameters derived from the measured s_u–z curve. It can be observed that the measured undrained shear strength generally increases with depth. The simulated s_u–z curves using the random field model are consistent with the measured s_u–z curve. Note that the variance of s_u, σ_{su}, increases significantly with depth. This result agrees well with Eq. (6) in which the σ_{su} is proportional to depth.

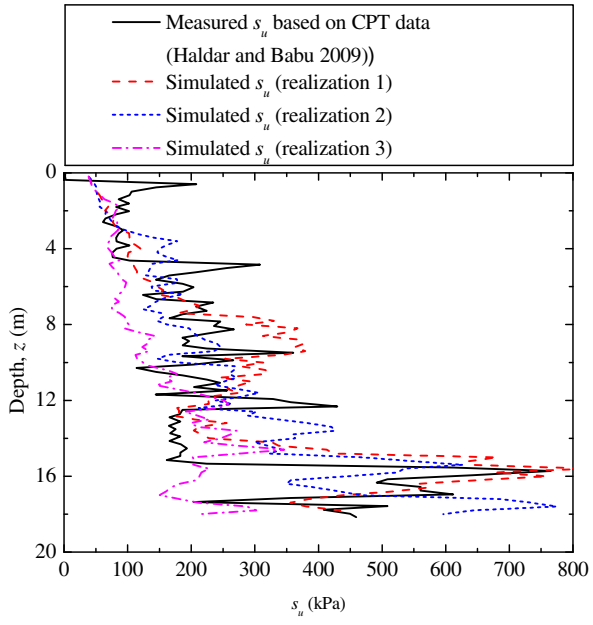

Fig. 3. Comparison between measured s_u–z curve and simulated s_u–z curves.

3.2. Simulation of effective friction angle

Following Phoon and Kulhawy [27], the spatial variation of the friction angle can be decomposed into a smoothly varying trend function, $t_\phi(z)$, and a fluctuating component, $w_\phi(z)$, as follows:

$$\phi(z) = t_\phi(z) + w_\phi(z) \tag{10}$$

where $\phi(z)$ is the friction angle and z is the depth. The fluctuating component represents inherent spatial (soil) variability. It is customary to assume that $w_\phi(z)$ is a zero-mean statistically homogeneous random field. The trend function can be viewed as the mean of the friction angle. Phoon et al. [28] and Baecher and Christian [3] suggested that the form of trend function should be the simplest one that would produce statistically homogeneous fluctuations. With this parsimonious principle in mind, a linear function is selected as the trend function of the friction angle:

$$t_\phi(z) = a_\phi z + b_\phi \tag{11}$$

in which a_ϕ is the rate of change of the mean friction angle with depth and b_ϕ is the mean value of the friction angle at the ground surface ($z = 0$). Values of a_ϕ are not widely reported in the literature. However, it is reasonable to estimate the value of a_ϕ from the ϕ-z curves shown in Fig. 2. These curves were derived using CPT data and an empirical correlation shown in Eq. (4). The values of a_ϕ estimated using these ϕ-z curves fall within the range of [0.24°/m, 2.38°/m]. Thus, a_ϕ within this range can be adopted to perform parameter analysis.

Similarly, the marginal distribution of ϕ is considered to be lognormal to avoid negative values. The mean and standard deviation of the natural logarithm ϕ are respectively given by:

$$\begin{cases} \lambda_{\ln\phi} = \ln(t_\phi) - 0.5\ln(1 + COV_\phi^2) \\ \xi_{\ln\phi} = \sqrt{\ln(1 + COV_\phi^2)} \end{cases} \tag{12}$$

in which $\lambda_{\ln\phi}$ and $\xi_{\ln\varphi}$ are the mean and standard deviation of the natural logarithm ϕ; t_ϕ is the mean of ϕ whose value is determined by the trend function shown in Eq. (11); COV_ϕ is the COV of ϕ which is the ratio of the standard deviation of $w_\phi(z)$ to t_ϕ. Unlike the standard deviation of undrained shear strength that increases linearly with depth (Eq. (6)), the standard deviation of $\phi(z)$, (or $w_\phi(z)$), at different depths are the same, because an additive model in the form of Eq. (10) has been adopted. The simulation steps are the same as those for the undrained shear strength. Moreover, the same autocorrelation function as $\ln(a)$, namely the single exponential autocorrelation function in Eq. (9), is adopted for $\ln(\phi)$.

Similarly, Fig. 4 shows the measured ϕ-z curve derived from CPT data reported in Singh and Chung [30] and the simulated ϕ-z curves using the parameters derived from the measured ϕ-z curve. There exists a general trend of the mean of friction angle increasing with depth. Additionally, the variance of ϕ is basically constant with depth even though the mean of ϕ increases with depth, because of the additive model (Eq. (10)).

It should be pointed out that two different random field models are adopted for modeling the spatial variability of undrained shear strength and friction angle. This is briefly explained as below. As pointed out by Lumb [25], there are three different forms of spatial variability for a soil parameter as shown in Fig. 5. Case 1 refers to the soil property v being normally distributed about the mean. Both the mean and standard deviation of v are constant with depth. Case 2 refers to v being normally distributed about a linear trend, and the variance of v is independent of depth. Case 3 represents the case that v is normally distributed about a linear trend and the variance of v increases with depth. It is evident from the in-situ data that the adopted spatial variability model of undrained shear strength in Section 3.1 corresponds to Case 3 in Fig. 5(c) while the

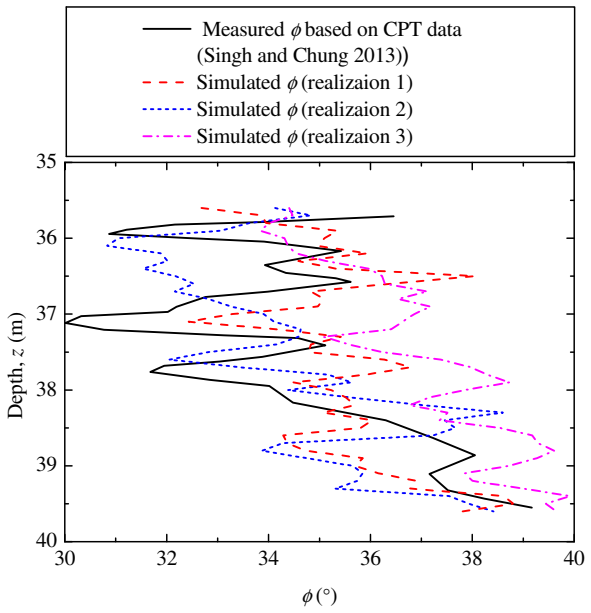

Fig. 4. Comparison between measured ϕ–z curve and simulated ϕ–z curves.

adopted spatial variability model of friction angle in Section 3.2 corresponds to Case 2 in Fig. 5(b). Hence, two different random field models are adopted here to obtain a linearly increasing standard deviation with depth for the undrained shear strength and a constant standard deviation with depth for the friction angle, respectively. The undrained shear strength is simulated through the relationship between s_u and a, i.e. Eq. (5). The spatial variability of s_u is transformed into the spatial variability of a [38]. The friction angle is simulated directly using the random field model in Eq. (10).

4. Reliability analysis of an infinite slope

The infinite slope model is one of the most popular models that is widely used in slope reliability analysis. For illustration, the infinite slope example studied by Griffiths et al. [13] is investigated again, which is shown in Fig. 6. In Fig. 6, H is the depth of soil above bedrock; z is the depth of the soil layer from ground to the potential slip line; β is the slope inclination; c and ϕ are the effective cohesion and friction angle at the base of the potential slip line, respectively; γ is the total unit weight; u is the pore pressure at the base of the potential slip line. The factor of safety, FS, is given by

$$FS = \frac{(z\gamma\cos^2\beta - u)\tan\phi + c}{z\gamma\sin\beta\cos\beta} \quad (z \leqslant H) \tag{13}$$

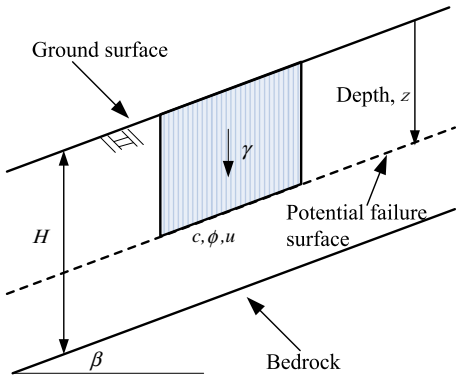

Fig. 6. An infinite slope model.

The performance function of slope reliability analysis is often expressed as $g(\mathbf{X}) = FS\text{-}1$, in which $\boldsymbol{X}$ represents the input random variables associated with slope reliability analysis. When FS is calculated using Eq. (13), the slope reliability can be readily evaluated using the FORM when all the six parameters in Eq. (13) are treated as random variables. An example of such an analysis is given by Griffiths et al. [13]. When spatially variable shear strength parameters are taken into consideration, the procedure for evaluating the infinite slope reliability is summarized as follows:

(1) The infinite slope can fail along a potential slip line running parallel to the ground surface at depth z. Two hundred potential slip lines are created by discretizing the soil depth into equal parts. Note that the choice of 200 potential slip lines is a reasonable compromise after performing parametric studies. In the illustrative example discussed below with $H = 5$ m, this implies generating potential slip lines at 25 mm intervals.
(2) The value of s_u for the undrained clay slopes or the value of ϕ for the sandy slopes at the base of each slip line is obtained from a KL expansion.
(3) The factor of safety for each slip line is calculated using Eq. (13). For the case that the soil column is modeled by 200 slip lines, this approach will produce 200 different factors of safety for the infinite slope. The minimum FS among the 200 factors of safety is taken as the "correct" value for the particular simulation, and its corresponding depth is the critical depth.
(4) The aforementioned procedure is repeated N times, i.e. the sample size of the Monte Carlo simulation is N. This approach will lead to N factors of safety for the infinite slope. Then, the probability of failure is calculated simply as the proportion of the number of results in which $FS < 1$ to N. Note that the accuracy in the probability of slope failure

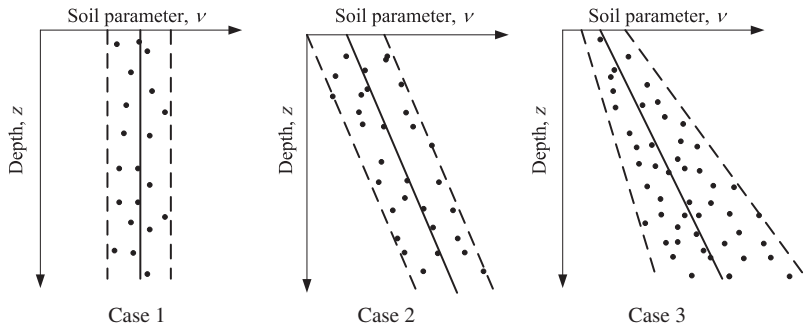

Fig. 5. Different forms of spatial variability for a soil parameter v with depth.

increases with increasing number of simulations. However, more computational efforts will be incurred because of more simulations. The choice of 200 slip lines is generally found to produce satisfactory results. To lead to sufficiently accurate reliability results, the required number of simulations should be more than 10^5 in this study.

5. Illustrative example

5.1. Infinite clay slope

The first infinite slope example considered here only treats s_u as a spatially varying random variable. Among the other five parameters in Eq. (13), the friction angle and pore water pressure are set to zero (the ground water table is assumed to be at or below the bottom of soil slope and the soil is saturated, i.e. $u = 0$), and parameters γ, H and β are constants. Then, Eq. (13) can be simplified as

$$FS = \frac{s_u}{z\gamma \sin\beta \cos\beta} \quad (z \leqslant H) \tag{14}$$

For illustration, the following parameters are adopted: $\gamma = 20$ kN/m^3, $H = 5$ m and $\beta = 30°$. Parameter a in Eq. (5) is assumed to be a lognormal distribution with a mean of 0.8 and a COV of 0.4. Parameter b in Eq. (5) is a constant with a value of 30 kPa. Based on these parameters, the mean and COV of s_u at the bottom of the slope, calculated by Eqs. (6) and (7), are obtained as 70 kPa and 0.23, respectively. The mean and COV of s_u at the mid-depth of the slope are 50 kPa and 0.16, respectively. Since the COV of s_u increases with depth as shown in Eq. (7), the maximum COV of $s_u = 0.23$ is found at the bottom of the slope. It falls within the typical range [0.1, 0.5] as reported in Phoon and Kulhawy [27]. These results indicate that the adopted value of $COV_a = 0.4$ is reasonable tentatively. For comparison, it is assumed that the mean and COV of s_u for the undrained shear strength constant with depth are the same as those at the mid-depth of the slope for the undrained shear strength linearly increasing with depth. This assumption is made due to the following reasons. If a set of spatially varying s_u data are treated using the constant trend model and the linear trend model respectively, the t_{su} for the constant trend model is the same as the t_{su} at the mid-depth of the slope for the linear trend model. Moreover, the COV of s_u derived from the linear trend model highly depends on the depth as shown in Eq. (7), whereas it is a constant for a constant trend model. For simplicity, the COV of s_u for the constant trend model is assumed to be the same as that at the mid-depth of the slope for the linear trend model. Under this assumption, the resulting mean and COV of s_u at the mid-depth of the slope are 50 kPa and 0.16, respectively. Eight values of $\triangle = l_v/H = 0.05$, 0.1, 0.2, 0.4, 0.8, 1.2, 1.6, and 2 are adopted in the parametric studies.

For comparison, Fig. 7(a) and (b) show typical realizations of random field of s_u for the t_{su} constant along depth and linearly increasing with depth, respectively. In these two figures, light colors represent low values of s_u, and dark colors represent high values of s_u. It can be seen from Fig. 7(a) that s_u at the bottom of the slice take high values because the t_{su} linearly increases with depth. While for the t_{su} constant with depth, s_u at the bottom of the slice may take low values, which is less realistic in comparison with the results in Fig. 1.

Table 1 shows the probabilities of failure for various correlation lengths. The probabilities of failure for the t_{su} linearly increasing with depth are significantly lower than those for the t_{su} constant with depth. For normalized correlation length $\Delta = 2$, the probabilities of failure are 0.40% for the t_{su} linearly increasing with depth and 20.84% for the t_{su} constant along depth, respectively. The latter is about 50 times the former. These results imply that the slope reliability will be underestimated greatly if the mean trend of s_u linearly increasing with depth is ignored. As expected, the probability of failure decreases with correlation length. Furthermore, it converges to a certain value as the correlation length becomes larger. This is consistent with the observation reported in Griffiths et al. [13].

Fig. 8(a) compares the factors of safety of the infinite slope for the t_{su} constant along depth with those for the t_{su} linearly increasing with depth. The factors of safety are computed using the mean value of the undrained shear strength. Generally, the factors of safety decrease with depth. Hence, the minimum factor of safety

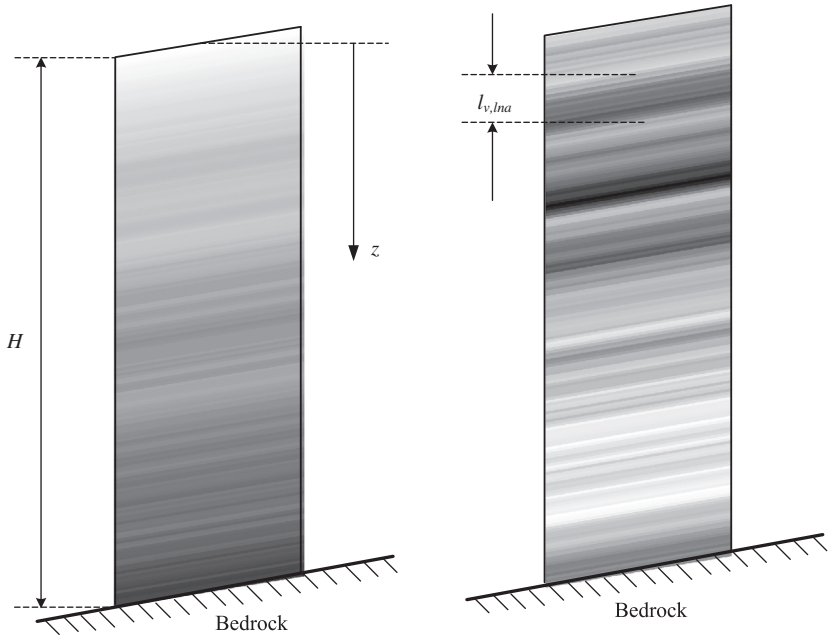

(a) t_{su} linearly increasing with depth (b) t_{su} constant with depth

Fig. 7. Typical realizations of random field of s_u.

Table 1
Probability of slope failure considering spatially varying undrained shear strength.

$\Delta = l_v/H$	0.05	0.1	0.2	0.4	0.8	1.2	1.6	2.0
$\mu_a = 0.8$	1.59%	1.12%	0.79%	0.59%	0.47%	0.45%	0.42%	0.40%
$\mu_a = 0$	57.02%	42.87%	33.14%	26.80%	23.31%	22.83%	21.93%	20.84%

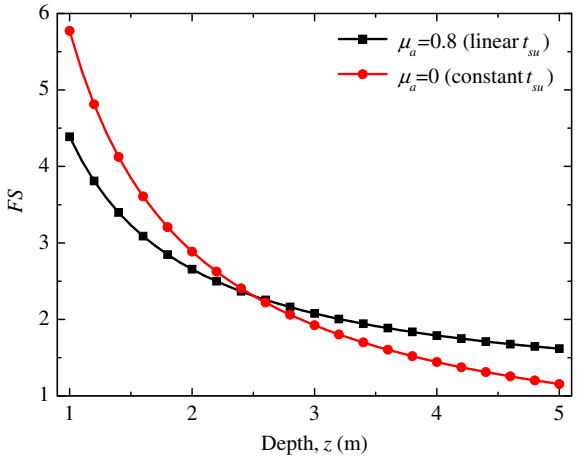

(a) *FS*

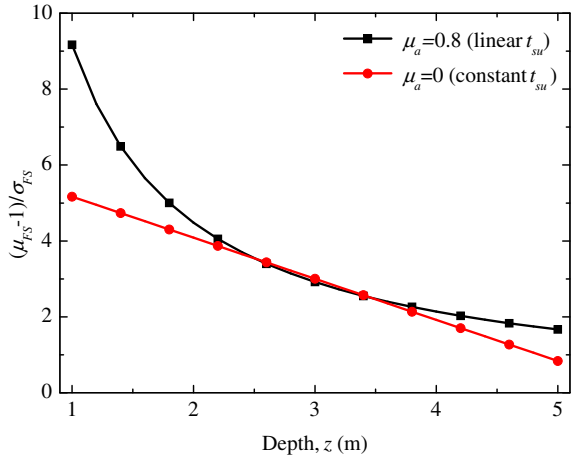

(b) $(\mu_{FS}-1)/\sigma_{FS}$

Fig. 8. Factor of safety and $(\mu_{FS}-1)/\sigma_{FS}$ of the infinite clay slope for various rates of change in t_{su}.

and the corresponding critical slip line occur at the base of the slope. This is because the factor of safety is proportional to the value of s_u/z (Eq. (14)) when the deterministic analysis is performed for the infinite slope. Since the t_{su} at the bottom of the slope for t_{su} linearly increasing with depth is higher than that for t_{su} constant with depth, the factor of safety for the former is larger than that for the latter. Meanwhile, the standard deviation of *FS* for the t_{su} linearly increasing with depth, $\sigma_{FS1}(z)$, can be derived as

$$\sigma_{FS1}(z) = \frac{COV_a \mu_a \gamma' z}{z\gamma \sin\beta\cos\beta} = \frac{COV_a \mu_a \gamma'}{\gamma \sin\beta\cos\beta} \tag{15}$$

It is evident that the resulting $\sigma_{FS1}(z)$ is constant with depth. Similarly, the standard deviation of *FS* for the t_{su} constant with depth, $\sigma_{FS2}(z)$, can be derived as

$$\sigma_{FS2}(z) = \frac{COV_a \mu_a \gamma'(0.5H)}{z\gamma \sin\beta\cos\beta} \tag{16}$$

Note that the resulting $\sigma_{FS2}(z)$ decreases with depth.

It is well known that the reliability index can be approximately calculated using $(\mu_{FS}-1)/\sigma_{FS}$, as shown in Fig. 8(b). It can be observed that the values of $(\mu_{FS}-1)/\sigma_{FS}$ decrease with depth for both cases. Moreover, the values of $(\mu_{FS}-1)/\sigma_{FS}$ for the t_{su} linearly increasing with depth are significantly larger than those for the t_{su} constant with depth. Consequently, the probability of slope failure for the t_{su} linearly increasing with depth is considerably smaller than that for the t_{su} constant with depth.

Taking the normalized correlation length $\Delta = 0.05$ as an example, the distribution of the depths of the critical slip line is plotted in Fig. 9. The frequency is calculated by the ratio of the number of critical slip lines at a specific depth to the total number of simulations, and the interval of depth is set as 0.1 m. Note that the critical depth is most likely to occur at the bottom of the slope whether the t_{su} linearly increases with depth or is constant with depth. For the

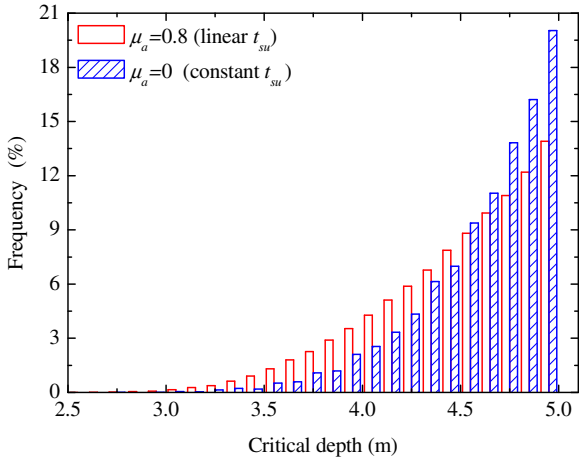

Fig. 9. Distribution of the depth of the critical slip line for various rates of change in t_{su} and $\triangle = 0.05$.

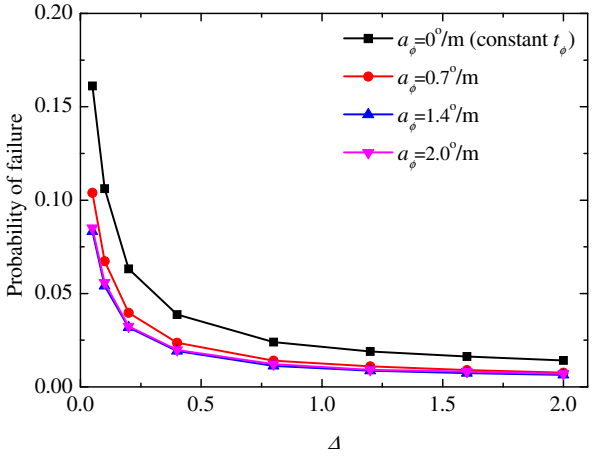

Fig. 10. Probability of failure of the infinite sand slope for various rates of change in t_{ϕ}.

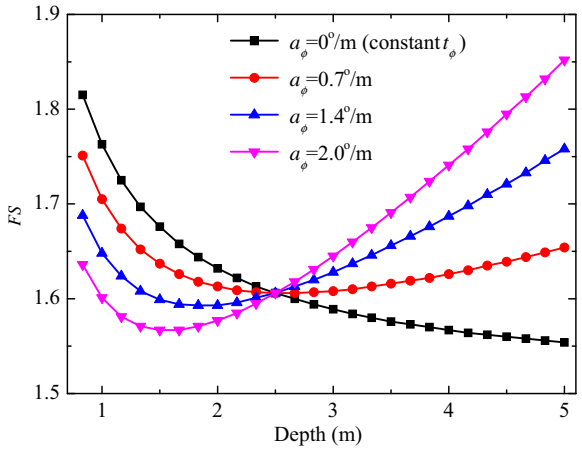

Fig. 11. Factor of safety of the infinite sand slope for various rates of change in t_ϕ.

t_{su} linearly increasing with depth, only about 14% of the critical slip lines occur at the base. This is because there is a greater probability of the minimum s_u/z occurring higher in the slope. In comparison with t_{su} constant along depth, the percentage of critical slip lines occurring at the base of the slope decreases as it is less likely that the minimum factor of safety occurs at the base of the slope. The reason is that the values of $(\mu_{FS}\text{-}1)/\sigma_{FS}$ at the bottom of the slope for the t_{su} linearly increasing with depth are slightly higher than those for the t_{su} constant with depth (see Fig. 8(b)).

5.2. Infinite sandy slope

In this section, the effect of spatially variable ϕ on slope reliability is illustrated using an infinite sandy slope where the ground water table is very deep, i.e. no pore water pressure is present at the base of potential slip lines. Only ϕ is modeled as a spatial variable. The other parameters are considered to be deterministic. The factor of safety in Eq. (13) can be further simplified as

$$FS = \frac{c}{z\gamma \sin\beta \cos\beta} + \frac{\tan\phi}{\tan\beta} \quad (z \leqslant H) \tag{17}$$

The following values are adopted: H = 5.0 m, β = 25°, γ = 20 kN/m^3, and c = 2 kPa. The friction angle follows a lognormal marginal distribution with a COV ϕ = 0.15. To account for ϕ varying with depth, a few linearly increasing trend functions are considered. Four sets of a_ϕ and b_ϕ parameters are considered: (0°/m, 35°), (0.7°/m, 33.25°), (1.4°/m, 31.5°), and (2.0°/m, 30°). The selection of a_ϕ has been discussed in Section 3.2. The t_ϕ is constant with depth when a_ϕ = 0°/m. Different values of b_ϕ are chosen here to ensure that the mean value of ϕ in the mid-depth of the slope is fixed at 35°.

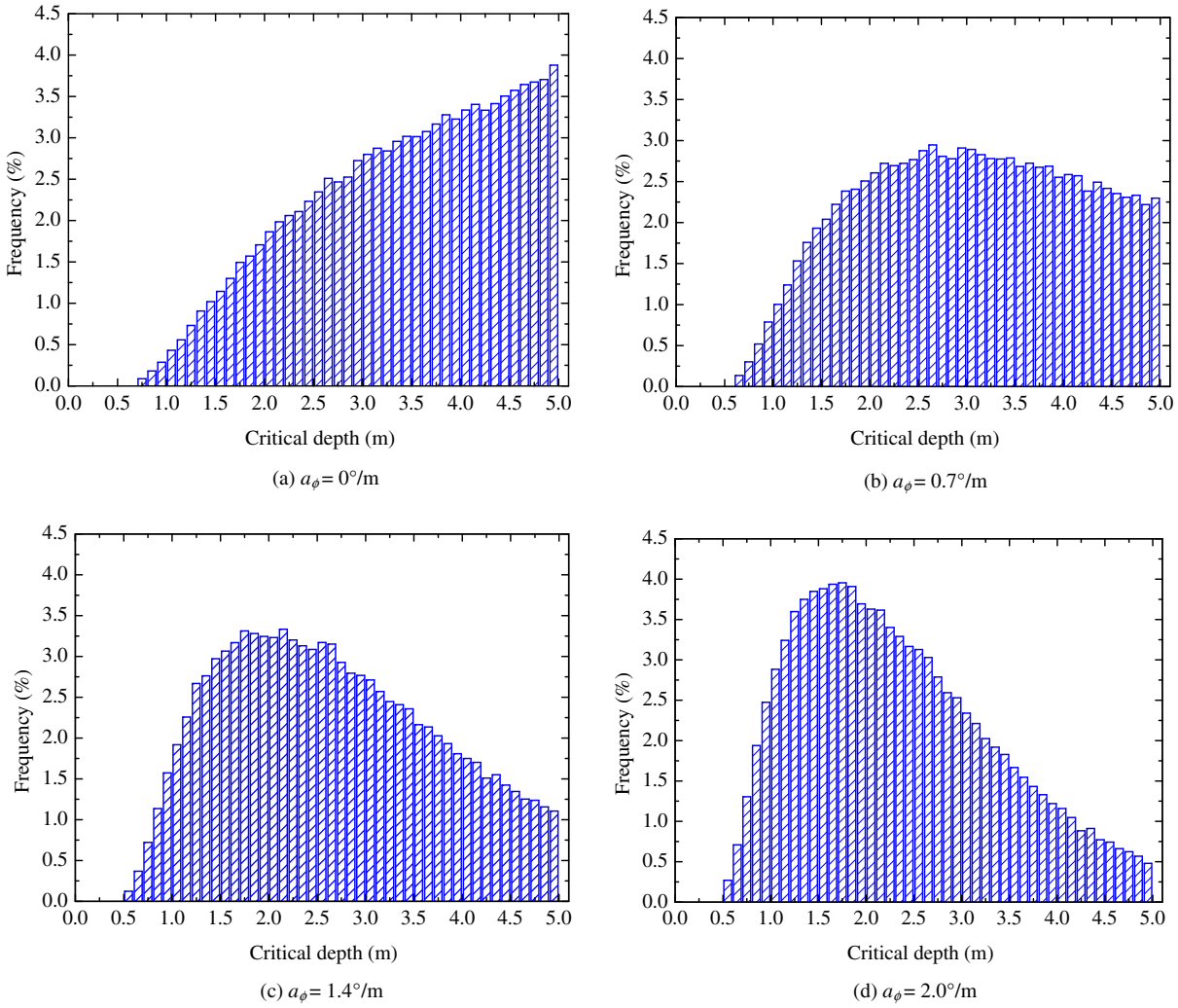

Fig. 12. Distribution of the depth of the critical slip line for △ = 0.05.

Fig. 10 shows the probabilities of slope failure for various rates of change in t_ϕ. As expected, the probability of slope failure decreases with correlation length. The probability of slope failure first decreases and then increases slightly with increasing a_ϕ. If the trend of the friction angle linearly increasing with depth is not taken into consideration, the probability of slope failure will be overestimated, which is conservative for slope safety assessment.

To explain the results in Fig. 10, the factors of safety of the sandy slope with various rates of change in t_ϕ are plotted in Fig. 11. Note that the factors of safety are computed using the mean values of the friction angle at the slip lines. Compared with the results in Fig. 8, the factors of safety do not monotonically decrease with depth. This is because when the friction angle is constant with depth or slightly increases with depth, the slope stability is mainly dominated by the depth of critical slip line. The minimum factor of safety still occurs at the base of the slip line due to the prior influence of the depth of critical slip line. However, when the friction angle significantly increases with depth, the slope stability is influenced by the cohesion, the friction angle and the depth of critical slip line simultaneously. Consequently, the minimum factor of safety does not necessarily occur at the base of the slip line. It should be noted that the variation of reliability index $(\mu_{FS}\text{-}1)/\sigma_{FS}$ is similar to that of μ_{FS} because the σ_{FS} is constant for various rates of change in t_ϕ and depths. Hence, the behavior of $(\mu_{FS}\text{-}1)/\sigma_{FS}$ with depth is similar to Fig. 11, which is not repeated again.

Fig. 12 shows the distribution of the depth of the critical slip line for $\Delta = 0.05$. The distribution of the depth of the critical slip line is significantly influenced by spatially varying friction angle. When the friction angle is constant with depth (see Fig. 12(a)), the critical slip line is most likely to occur at the bottom of the slope, such observation is consistent with Fig. 9 associated with the undrained slope. When the friction angle increases slightly with depth (see Fig. 12(b)), the distribution of the depth of the critical slip line displays a rather uniform frequency at the medium and bottom of the slope (see Fig. 12(b)). When the friction angle increases greatly with depth, the depth of the critical slip line is most likely to occur at the mid-depth of the slope (see Fig. 12(c)) or at the top of the slope (see Fig. 12(d)). These results clearly indicate that if the trend of friction angle increasing with depth is ignored, a less reasonable conclusion that the critical slip line occurs at the bottom of the slope will be drawn.

5.3. Discussion

It is well known that the cohesion and friction angle are negatively correlated. The Mohr-Coulomb failure envelope is generally nonlinear and this negative correlation between cohesion (y-intercept) and friction angle (gradient) is an outcome of fitting a linear line to this failure envelope (e.g., [27,8,13,21]). Hence, the cohesion and friction angle should be modeled as a correlated vector field from a physical point of view. In this study, the cohesion is assumed to be deterministic (c = 2 kPa) due to the following reasons:

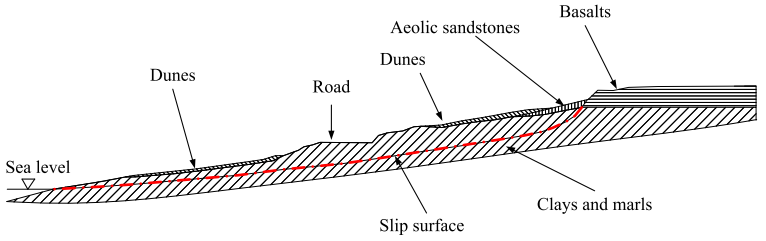

(a) Murru Mannu land slide (Canuti et al. [4])

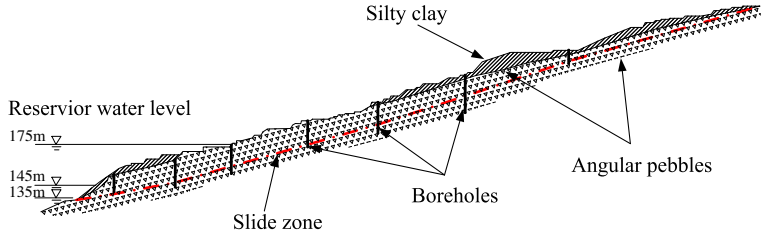

(b) Majiagou landslide (Li et al. [23])

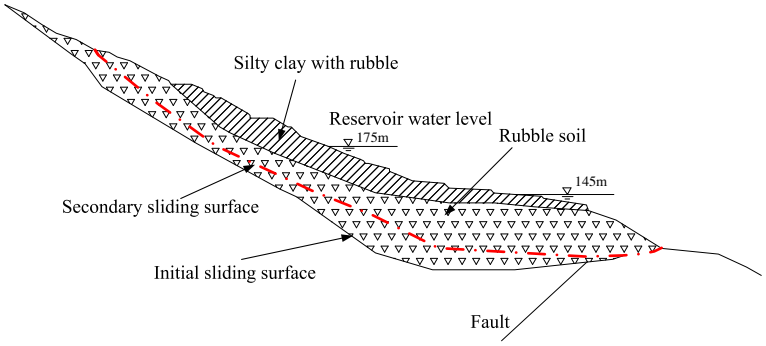

(c) Bazimen landslide (Du et al. [9])

Fig. 13. Landslides in reality.

(1) The in-situ data related to the shear strength parameters varying with depth are limited in geotechnical engineering practice. The trend function for the undrained shear strength or friction angle is determined through the empirical relation between them and in-situ data obtained from CPT or SPT. For cohesive soil, such an empirical relation is often used to estimate the undrained shear strength. For cohesionless soil, such an empirical relation is used to estimate friction angle. To the best of our knowledge, there is no empirical relation to estimate cohesion and friction angle simultaneously based on in-situ data. Hence, the trend functions for cohesion and friction angle cannot obtained simultaneously from a practical point of view although the trend functions for negatively correlated shear strength parameters can be obtained theoretically.

(2) If the assumed trend functions for cohesion and friction angle are used and a negative correlation coefficient of $\rho = -0.5$ between cohesion and friction angle is imposed on the detrended fluctuations, the slope reliability results can also be obtained using the proposed method. It is found that the negative correlation between cohesion and friction angle has a slight effect on the depth of the critical slip line, i.e. results similar to Fig. 12 are obtained. The probability of slope failure will be reduced significantly when the negative correlation between cohesion and friction angle is taken into consideration, but the trend is similar to Fig. 10. This observation is consistent with those made in many past studies (e.g., [8,13,34]).

6. Cases of shallow landslides

The probability of failure and the depth of critical slip line of the infinite slopes in the presence of spatially varying shear strength parameters that linearly increase with depth have been studied. In this section, several typical shallow landslides reported in the literature [4,9,23] are collected to assess the above results. The three considered landslides are listed as follows: Murru Mannu landslide in Western Sardinia, Italy [4], Majiagou landslide [23] and Bazimen landslide [9] in the Three Gorges Reservoir Region, China. The landslide profiles are shown in Fig. 13. Note that the sliding surfaces associated with the three landslides are all parallel to the slope surface. Moreover, the length-to-depth ratios of the landslide mass are extremely large. These characters are consistent with the shallow landslides that are often simplified as the infinite slopes. Additionally, all the sliding surfaces pass through statistically homogeneous soils rather than the base of homogeneous soils. These results further demonstrate that the critical slip surface underlying the infinite slope does not necessarily occur at the bottom of slope, which is consistent with the observation obtained from this study. Hence, a realistic assessment of slope safety should consider the non-constant mean trend of shear strength parameters. Otherwise, misleading results associated with slope reliability analysis may be obtained.

7. Conclusions

The reliability of infinite slopes in the presence of spatially varying shear strength parameters that linearly increase with depth is studied. The KL expansion is adopted to discretize the random fields of spatially varying shear strength parameters. The following conclusions are drawn based on illustrative examples:

(1) The mean trend of the shear strength parameters has a significant influence on slope reliability. The probability of slope failure will be overestimated if a linearly increasing trend underlying the shear strength parameters is ignored or simplified as a constant trend.

(2) The critical slip line in an infinite clay slope is most likely to occur at the bottom of the slope even though the trend of the undrained shear strength is considered. Compared with the undrained shear strength constant with depth, the possibility of critical slip lines occurring at the bottom of the slope decreases considerably in the presence of linearly increasing mean trend.

(3) The mean trend of the friction angle has a considerable influence on the distribution of the critical failure depths of an infinite sandy slope. The most likely critical failure line does not occur at the bottom of the slope when the mean trend is increasing with depth. It can occur at the mid-depth or at the top of the infinite slope.

Acknowledgments

This work was supported by the National Science Fund for Distinguished Young Scholars (Project No. 51225903) and the National Basic Research Program of China (973 Program) (Project No. 2011CB013506) and the National Natural Science Foundation of China (Project No. 51329901).

References

[1] Ahmed A, Soubra A-H. Probabilistic analysis of strip footings resting on a spatially random soil using subset simulation approach. Georisk 2012;6(3):188–201.
[2] Asaoka A, A-Grivas D. Spatial variability of the undrained strength of clays. J Geotech Eng Div ASCE 1982;108(5):743–56.
[3] Baecher GB, Christian JT. Spatial variability and geotechnical reliability. In: Phoon KK, editor. Reliability-based design in geotechnical engineering: computations and applications. London and New York: Taylor & Francis; 2008. p. 76–133.
[4] Canuti P, Casagli N, Fanti R. Slope instability conditions in the archaeological site of Tharros (Western Sardinia, Italy). In: Sassa K, Fukuoka H, Wang F, Wang G, editors. Landslides: risk analysis and sustainable disaster management. New York: Springer; 2005. p. 187–95.
[5] Cherubini C, Vessia G. Reliability-based pile design in sandy soils by CPT measurements. Georisk 2010;4(1):2–12.
[6] Ching JY, Phoon KK. Mobilized shear strength of spatially variable soils under simple stress states. Struct Saf 2013;41:20–8.
[7] Ching JY, Phoon KK. Probability distribution for mobilised shear strengths of spatially variable soils under uniform stress states. Georisk 2013;7(3):209–24.
[8] Cho SE. Probabilistic assessment of slope stability that considers the spatial variability of soil properties. J Geotech Geoenviron Eng 2010;136(7):975–84.
[9] Du J, Yin K, Lacasse S. Displacement prediction in colluvial landslides, Three Gorges Reservoir, China. Landslides 2013;10(2):203–18.
[10] Elkateb T, Chalaturnyk R, Robertson PK. Simplified geostatistical analysis of earthquake-induced ground response at the wildlife site, California, U.S.A. Can Geotech J 2003;40(1):16–35.
[11] Foye KC, Abou-Jaoude GG, Salgado R. Limit states design (LSD) for shallow and deep foundations. Report, Joint Transportation Research Program. West Lafayette (Indiana): Indiana Department of Transportation and Purdue University; 2004. Report No.: FHWA/IN/JTRP-2004/21.
[12] Griffiths DV, Fenton GA. Probabilistic slope stability analysis by finite elements. J Geotech Geoenviron Eng 2004;130(5):507–18.
[13] Griffiths DV, Huang JS, Fenton GA. Probabilistic infinite slope analysis. Comput Geotech 2011;38(4):577–84.
[14] Haldar S, Sivakumar Babu GL. Design of laterally loaded piles in clays based on cone penetration test data: a reliability-based approach. Geotechnique 2009;59(7):593–607.
[15] Hicks MA, Samy K. Influence of heterogeneity on undrained clay slope stability. Q J Eng Geol Hydroge 2002;35(1):41–9.
[16] Hicks MA, Spencer WA. Influence of heterogeneity on the reliability and failure of a long 3D slope. Comput Geotech 2010;37(7–8):948–55.
[17] Ji J, Liao HJ, Low BK. Modeling 2-D spatial variation in slope reliability analysis using interpolated autocorrelations. Comput Geotech 2012;40:135–46.
[18] Kulatilake PHSW, Um JG. Spatial variation of cone tip resistance for the clay site at Texas A&M University. Geotech Geol Eng 2003;21(2):149–65.

[19] Kulhawy FH, Mayne PW(Cornell University, Geotechnical engineering group). In: Manual on estimating soil properties for foundation design, Final report. Palo Alto (CA): Electric Power Research Institute; 1990. Report No.: EL-6800.
[20] Lacasse S, Nadim F. Uncertainties in characterizing soil properties. In: Proceeding of Uncertainty 1996. ASCE; Madison, Wisconsin; 1996.
[21] Li DQ, Chen YF, Lu WB, Zhou CB. Stochastic response surface method for reliability analysis of rock slopes involving correlated non-normal variables. Comput Geotech 2011;38(1):58–68.
[22] Li DQ, Wu SB, Zhou CB, Phoon KK. Performance of translation approach for modeling correlated non-normal variables. Struct Saf 2012;39:52–61.
[23] Li T, Zhang C, Xu P, Li P. Stability assessment and stabilizing approaches for the Majiagou landslide, undergoing the effects of water level fluctuation in the Three Gorges Reservoir area. In: Wang F, Li T, editors. Landslide disaster mitigation in Three Gorges Reservoir. China, New York: Springer; 2009. p. 331–52.
[24] Low BK, Lacasse S, Nadim F. Slope reliability analysis accounting for spatial variation. Georisk 2007;1(4):177–89.
[25] Lumb P. The variability of natural soils. Can Geotech J 1966;3(2):74–97.
[26] Luo XF, Li X, Zhou J, Cheng T. A Kriging-based hybrid optimization algorithm for slope reliability analysis. Struct Saf 2012;34(1):401–6.
[27] Phoon KK, Kulhawy FH. Characterization of geotechnical variability. Can Geotech J 1999;36(4):612–24.
[28] Phoon KK, Quek ST, An P. Identification of statistically homogeneous soil layers using modified Bartlett statistics. J Geotech Geoenviron Eng 2003;129(7):649–59.
[29] Rahardjo H, Satyanaga A, Leong EC, Ng YS, Pang HTC. Variability of residual soil properties. Eng Geol 2012;141–142:124–40.
[30] Singh VK, Chung SG. Shear strength evaluation of lower sand in Nakdong river delta. Mar Georesour Geotec 2013;31(2):107–24.
[31] Sivakumar Babu GL, Srivastava A, Murthy DSN. Reliability analysis of the bearing capacity of a shallow foundation resting on cohesive soil. Can Geotech J 2006;43(2):217–23.
[32] Srivastava A, Sivakumar Babu GL. Effect of soil variability on the bearing capacity of clay and in slope stability problems. Eng Geol 2009;108(1–2):142–52.
[33] Tang XS, Li DQ, Chen YF, Zhou CB, Zhang LM. Improved knowledge-based clustered partitioning approach and its application to slope reliability analysis. Comput Geotech 2012;45:34–43.
[34] Tang XS, Li DQ, Rong G, Phoon KK, Zhou CB. Impact of copula selection on geotechnical reliability under incomplete probability information. Comput Geotech 2013;49:264–78.
[35] Vanmarcke EH. Random fields: analysis and synthesis. Revised and expanded new edition. Beijing: World Scientific Publishing; 2010.
[36] Wilson DW, Abbo AJ, Sloan SW, Lyamin AV. Undrained stability of a circular tunnel where the shear strength increases linearly with depth. Can Geotech J 2011;48(9):1328–42.
[37] Wilson DW, Abbo AJ, Sloan SW, Lyamin AV. Undrained stability of a square tunnel where the shear strength increases linearly with depth. Comput Geotech 2013;49:314–25.
[38] Wu SH, Ou CY, Ching J, Juang CH. Reliability-based design for basal heave stability of deep excavations in spatially varying soils. J Geotech Geoenviron Eng 2012;138(5):594–603.
[39] Zhang J, Ellingwood B. Orthogonal series expansions of random fields in reliability analysis. J Eng Mech ASCE 1994;120(12):2660–77.
[40] Zhu H, Zhang LM. Characterizing geotechnical anisotropic spatial variations using random field theory. Can Geotech J 2013;50(7):723–34.
[41] Zhu H, Zhang LM, Zhang LL, Zhou CB. Two-dimensional probabilistic infiltration analysis with a spatially varying permeability function. Comput Geotech 2013;48:249–59.